Pergamon

Int. J. Heat Mass Transfer. Vol. 37, No. 11, pp. 1593–1603, 1994

0017-9310/94 $7.00+0.00

0017-9310(94)E0010-R

Conjugate heat transfer and particle deposition in the modified chemical vapor deposition process: effects of torch speed and solid layer

K. S. PARK and M. CHOI†

Seoul National University, Department of Mechanical Engineering, San 56-1 Shinrimdong, Kwanak-Ku, Seoul 151-742, Korea

(*Received* 15 *October* 1992 *and in final form* 10 *December* 1993)

Abstract—A study has been carried out for the conjugate heat transfer and particle deposition that occur during the modified chemical vapor deposition (MCVD) process. The analysis includes thermophoretic particle transport in the gas flow and heat transfer through the solid layer; the effects of variable properties in both the gas and the solid regions are included. A notable feature of the study is the inclusion of the effects of periodic heating due to the repeated traversing of the torch and the effects of the increasing solid layer thickness as the particles deposit. A new concept uses a two torch formulation to simulate the torch heating from both the present and the previous passes. This formulation is able to predict the minimum wall temperature in front of the torch, which is closely related to the deposition efficiency. Localized heating of the moving torch is studied using the heat flux boundary condition on the tube wall. The calculated surface temperature distribution and the deposition efficiency are in good agreement with experimental data. Of particular interest are the effects of torch speed and solid layer thickness on the efficiency, the rate of deposition of the particles and the taper length.

INTRODUCTION

A STUDY has been made of the particle deposition that occurs during the modified chemical vapor deposition (MCVD) process [1–3]. In the MCVD process which is currently utilized to manufacture high quality optical fibers, chemical reagents flow in a rotating fused silica tube which is heated by a traversing oxy–hydrogen torch. As the torch moves in the axial direction, the gases are heated and chemical reactions result in the formation of glassy particles which deposit on the inner surface of the tube. When the torch traverses the tube, a glassy film is deposited and many traverses (and layers) are needed to obtain the desired variation of the refractive index (high refractive index in the core and low refractive index in the cladding). After the desired layers are obtained, the tube is collapsed into a solid rod which is called a preform of the optical fiber. The preform is then drawn to produce the typical 125 μm diameter optical fiber. In the MCVD process, particle deposition results from thermophoresis; that is, from the net force that a suspended particle experiences in the direction of decreasing temperature [4, 5].

Walker *et al.* [4] studied numerically and experimentally the thermophoretic particle transport. Laser enhanced MCVD was investigated by Wang *et al.* [6] and Morse *et al.* [7]. A study of chemical kinetics and silica aerosol dynamics has been carried out by Kim and Pratsinis [8]. Three dimensional effects due to tube rotation and buoyancy have been studied by Choi *et al.* [9] and Lin *et al.* [10, 11].

Most studies have not considered the effects of torch speed and the solid layer on particle deposition in the MCVD process. However, in view of the importance of torch velocity and heating profile control in fiber manufacturing, the optimization of the process requires the proper understanding of these inputs. The solid layer includes the original tube wall and the deposited layer. In the present work, the effects of the velocity of the traversing torch and the solid layer thicknesses on the deposition of particles are studied. The repeated traversing of the torch along the fused silica tube causes the periodic heating which results in the existence of a minimum wall temperature ahead of the torch which was experimentally observed by Walker *et al.* [4]. The minimum wall temperature ahead of the torch was shown to be an important parameter for the evaluation of the deposition efficiency (Walker *et al.* [4]). Therefore, it is desirable for the optimization of the process to predict the wall temperature distributions for different operation conditions, especially, different torch speeds and solid layer thicknesses. The present study develops a model to predict the distributions of wall temperature as well

† To whom correspondence should be addressed.

NOMENCLATURE

c_p, c_{solid}	specific heats at constant pressure of gas and solid
E	deposition efficiency
h	heat transfer coefficient
k, k_{solid}	thermal conductivities of gas and solid
n	refractive index
q_{wall}	wall heat flux
q_{max}	maximum wall heat flux
r	radial coordinate
R_i	inner radius of the tube
R_o	outer radius of the tube
t	time
T	temperature
T_{max}	maximum wall temperature
T_e	equilibrium temperature
T_{min}	minimum outer wall temperature ahead of the torch
T_{rxn}	chemical reaction temperature
T_∞	ambient temperature
u	axial velocity
U_{av}	mean velocity of gas
V_{torch}	torch speed.

Greek symbols

α	Rosseland mean absorption coefficient
λ	parameter for a Gaussian heat flux distribution
μ	viscosity
ξ	axial coordinate
ξ_{torch}	axial location of the torch
ρ, ρ_{solid}	density of gas and solid
σ	Boltzmann constant.

as heat transfer and particle deposition in a gas flow for different operating conditions. The model includes the effects of the periodic heating and the heat transfer through the solid layer. The localized heating of the moving torch is described by a heat flux boundary condition on the tube wall instead of the wall temperature boundary condition previously used. The present calculations of the wall temperature distribution and the overall efficiency of particle deposition are compared with the experimental data [4] and shown to be in good agreement. Of particular interest are the effects of torch speeds and solid layer thicknesses on the efficiency, the rate of particle deposition, and the taper length.

ANALYSIS

The mixture of chemical reagents flows in the rotating tube of inner and outer radii R_i and R_o, respectively, as shown in Fig. 1. It has been shown [11] for small rotational speeds that the three dimensional effects due to buoyancy and tube rotation are important for the variation of the particle deposition in the circumferential direction, but are not important for either the axial variation of deposition or for the deposition efficiency. Normal operating speeds for tube rotation (60–120 r.p.m.) result in almost uniform deposition in the circumferential direction [11]. Walker *et al.* [4] neglected three dimensional effects and obtained efficiencies which were in good agreement with the experimental data. The major interest of the present work is the determination of the axial deposition profile for different torch velocities and solid layer thicknesses. Accordingly, tube rotation and buoyancy are neglected. From the above results, the axisymmetric, two dimensional variable property flow is considered. Temperature dependent properties are obtained from Weast and Astle [12] and Irvine and Liley [13]. The present work involves a complex coupled heat transfer problem including conduction in the solid layer and convection in the tube in order to determine the unknown wall temperature distribution.

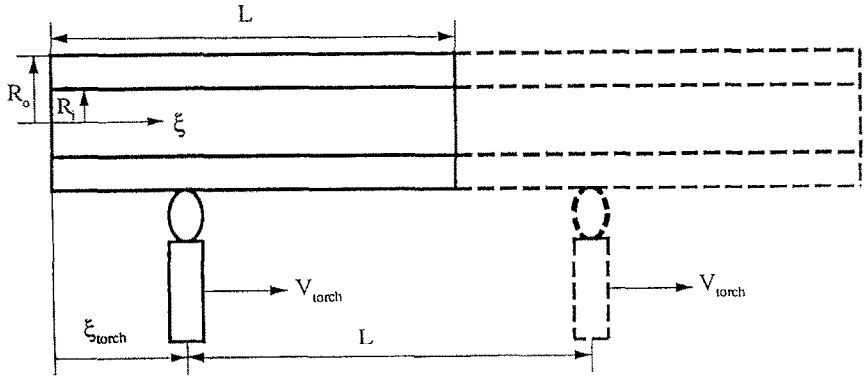

FIG. 1. Sketch of the system.

Utilizing a moving coordinate ξ defined by $\xi = x - V_{\text{torch}}t$, and assuming quasi-steady state conditions, the governing equations in cylindrical coordinates (r, ξ) for the gas flow inside the tube are:

continuity

$$\frac{\partial(\rho u)}{\partial \xi} + \frac{1}{r}\frac{\partial(\rho r v)}{\partial r} = 0 \tag{1}$$

momentum

$$\rho\left(u\frac{\partial u}{\partial \xi} + v\frac{\partial u}{\partial r}\right) = -\frac{\partial p}{\partial \xi} + \left(\frac{\partial \tau_{\xi\xi}}{\partial \xi} + \frac{1}{r}\frac{\partial(r\tau_{\xi r})}{\partial r}\right) \tag{2a}$$

$$\rho\left(u\frac{\partial v}{\partial \xi} + v\frac{\partial v}{\partial r}\right) = -\frac{\partial p}{\partial r} + \left(\frac{\partial \tau_{\xi r}}{\partial \xi} + \frac{1}{r}\frac{\partial(r\tau_{rr})}{\partial r} - \frac{\tau_{\theta\theta}}{r}\right) \tag{2b}$$

energy

$$\rho c_p\left(u\frac{\partial T}{\partial \xi} + v\frac{\partial T}{\partial r}\right) = \frac{\partial}{\partial \xi}\left(k\frac{\partial T}{\partial \xi}\right) + \frac{1}{r}\frac{\partial}{\partial r}\left(kr\frac{\partial T}{\partial r}\right) \tag{3}$$

where

$$\tau_{\xi\xi} = \mu\left[2\frac{\partial u}{\partial \xi} - \frac{2}{3}(\nabla \cdot V)\right], \quad \tau_{rr} = \mu\left[2\frac{\partial v}{\partial r} - \frac{2}{3}(\nabla \cdot V)\right],$$

$$\tau_{\xi r} = \mu\left[\frac{\partial u}{\partial r} + \frac{\partial v}{\partial \xi}\right], \quad \tau_{\theta\theta} = \mu\left[2\frac{v}{r} - \frac{2}{3}(\nabla \cdot V)\right]. \tag{4}$$

The boundary conditions are:

$$\text{at } \xi = -\infty, \quad u = 2U_{\text{av}}\left(1 - \left(\frac{r}{R_i}\right)^2\right) - V_{\text{torch}},$$

$$v = 0, \quad T = T_\infty \tag{5a}$$

$$\text{at } \xi = \infty, \quad \frac{\partial(u, v, T)}{\partial \xi} = 0 \tag{5b}$$

$$\text{at } r = 0, \quad u, v, T \text{ are finite} \tag{5c}$$

$$\text{at } r = R_i, \quad u = -V_{\text{torch}}, \quad v = 0$$

and continuity of temperature and heat flux. (5d)

Heat conduction occurs through the solid layer which consists of both the original tube wall and the deposited layer. The energy equation in the solid region is given by:

$$(\rho c)_{\text{solid}}(-V_{\text{torch}})\frac{\partial T}{\partial \xi} = \frac{\partial}{\partial \xi}\left(k_{\text{solid}}\frac{\partial T}{\partial \xi}\right) + \frac{1}{r}\frac{\partial}{\partial r}\left(k_{\text{solid}} r\frac{\partial T}{\partial r}\right). \tag{6}$$

Another consideration is the effect of the torch heating from the previous pass. In the real process, after one pass is completed, the torch returns to the starting position (i.e. $\xi = 0$ in Fig. 1) and repeats the traverse. If a single torch formulation is used, the tube wall ahead of the present torch (i.e. the solid torch in Fig. 1) cannot experience heating by the torch (the regions behind the torch have of course been heated by the present torch). Accordingly, in single torch studies, wall temperatures for $\xi > \xi_{\text{torch}}$ become equal to the ambient temperature except in the regions very near the torch. However, in the real case, the regions ahead of the present torch were heated by the torch from the previous pass and the wall should be at higher temperatures than the ambient. Walker *et al.* [4] experimentally found that the wall temperature decreased rapidly ahead of the present torch, but increased gradually after the minimum value was reached. This is the result of the torch heating from the previous pass. To simulate the effects of the torch heating from both the present pass and the previous pass, a two torch model is developed for the first time (two torches are considered to be moving at the same speed and are separated by a distance of one tube length, Fig. 1). The dashed torch causes the heating that occurred from the previous pass and the solid torch represents the heating from the present pass. In the quasi-steady condition, the heating (and temperature) profiles are related to the moving torch and the axial distance measured from the torch determines the elapsed time after the torch heating. Therefore, the regions farther behind the torch cool down for a longer time and accordingly, have lower wall temperatures than the regions that are nearer and behind the torch. The regions ahead of the present torch were not heated by the present (solid) torch, but were heated by the previous (dashed) torch heating. Depending on the distance from the dashed torch, the elapsed time (and cooling time) is determined from the torch heating of the previous pass. For example, the regions near the right end of the tube ($\xi = L$) cool for a shorter time after the torch heating of the previous pass than the regions near and ahead of the present torch. Accordingly, the regions near $\xi = L$ may have a higher wall temperature than the regions that are near and ahead of the present torch. In summary, the two torch concept with the tube extension clarifies the heating effects from the previous pass. Comparisons of the wall temperatures between the calculations using the two torch concept and the experimental data are shown later. The localized heating of each torch is modelled using a heat flux boundary condition on the tube wall instead of the specified wall temperature boundary condition which has been used in most studies of the MCVD process; q_{wall} is given by

$$q_{\text{wall}} = q_{\max}\exp\left(-10\,000\lambda^2(\xi - \xi_{\text{torch}})^2\right) + q_{\max}\exp\left(-10\,000\lambda^2(\xi - (L + \xi_{\text{torch}}))^2\right) = k_{\text{solid}}\frac{\partial T}{\partial r} + h(T)(T - T_\infty) \quad \text{at } r = R_o \tag{7}$$

where ξ_{torch} is the torch location of the present pass (solid torch) and $L + \xi_{\text{torch}}$ is the torch location of the previous pass (dashed torch). Temperature dependent

heat transfer coefficient data, $h(T)$, are given by Farouk and Ball [14] and Gardon [15].

Two parameters, λ and q_{max}, are needed to specify a given torch heating condition. The value of λ characterizes the width of the heating profile; e.g. small λ represents broad heating and large λ represents narrow heating. The parameter, q_{max}, is the maximum heat flux which is dependent on the flow rate of the fuel. A major advantage of this boundary condition is that it may be utilized for different torch speeds; previous approaches which use the wall temperature require measurements of the wall temperature for the specific torch speed being studied. Another advantage (shown later) is that the minimum wall temperature, T_{min}, ahead of the torch, which is closely related to the overall efficiency of particle deposition, i.e. $E = 0.8(1 - T_{min}/T_{rxn})$ as given by Walker *et al.* [4], can now be predicted. In the previous models T_{min} depends on the measurement of outside wall temperatures. It is emphasized that the occurrence of the minimum wall temperature ahead of the torch results from the periodic heating of the torch and the resulting heat transfer through the solid layer.

In studies of optical fiber drawing, Paek and Runk [16] and Homsy and Walker [17] included the effect of radiation in a silica solid by using the Rosseland diffusion approximation [18]. In the solid layer of the silica tube of the present study, the same approximation is utilized. Note that the fused silica can be considered to be opaque for photons with wavelengths larger than approximately 5 μm, mildly opaque in the range 2.8–4.4 μm and transparent for wavelengths smaller than 2.8 μm [17]. This approximation may not always be valid. For a more complete study the integro–differential equation of radiative transfer should be utilized, but this is beyond the scope of the present investigation.

In the present formulation and that of refs. [16, 17],

$$k_{solid} = k_{conduction} + \frac{16n^2\sigma T^3}{3\alpha} \tag{8}$$

where n is the index of refraction ($n = 1.5$) and α is the Rosseland mean absorption coefficient ($\alpha = 4$ cm^{-1} [17]). It is noted that the previous studies which utilized equation (8) were for studies of the drawing of optical fibers.

Near the torch, the gas temperature exceeds the chemical reaction temperature T_{rxn} (Walker *et al.* [4]) and particles are formed. It is assumed that the chemical reaction is completed when the gas temperature reaches T_{rxn}. The motion of the particles is determined from the combined effects of flow velocity and thermophoresis, i.e.

$$\frac{d\xi}{dt} = u - \frac{Kv}{T}\frac{\partial T}{\partial \xi}, \quad \frac{dr}{dt} = v - \frac{Kv}{T}\frac{\partial T}{\partial r} \tag{9}$$

where $d\xi/dt$, dr/dt are the axial and radial velocities of the particles, respectively. A value of 0.9 [4] is used for K. It is emphasized that Brownian diffusion can be neglected in the MCVD process [5].

Numerical calculations have been performed using the finite volume technique using the SIMPLER algorithm [19]. Calculations using constant properties were first performed and compared with the analytical solution given in Lin *et al.* [20] and shown to be in good agreement. For the convective terms, a second order upwind differencing scheme is used and a bulk pressure correction is utilized to enhance the convergence rate. Grid sensitivity tests were carried out for several grid systems of (13×137), (15×200) and (26×274) and the (15×200) grid was determined to produce grid independent results within 2% for the wall temperature and the overall deposition efficiency. Further numerical details are described in Lin *et al.* [10].

RESULTS AND DISCUSSION

Results from the present study are compared with the experimental data of Walker *et al.* [4]. It is emphasized that the outer wall temperature, $T(r = R_o, \xi)$, is unknown *a priori*; $T(r = R_o, \xi)$ is determined by solving the energy conservation equations in the gas, equations (1)–(3), and the energy equation in the solid, equation (6) subject to the specified boundary conditions including the condition given in equation (7). The value of q_{max} in equation (7) essentially determines the maximum outer wall temperature, T_{max}, while λ characterizes the axial variation of the wall temperature and is related to the torch configuration. Comparisons in Fig. 2 with the experimental data of Walker *et al.* [4] for a tube of ID = 14 mm and OD = 16 mm show good agreement with values of $q_{max} = 6.50 \times 10^5$ W m^{-2} and $\lambda = 0.5$. It is emphasized that these values of q_{max} and λ can be used even for other operating conditions; e.g. different torch speeds, different solid layer thicknesses, etc. since the torch heating profile is unchanged for the same torch configuration and fuel rate. Recall that previous studies that use the wall temperature boundary condition must specify different wall temperatures for different torch speeds and solid layer thicknesses; this requires additional measurements of the wall temperatures which have not been reported.

The moving torch results in a non-symmetric wall temperature distribution (even with a symmetric flux variation with respect to the moving torch). This can be seen by considering the reference frame that is moving with the torch. The moving wall approaches the stationary torch ($\xi = 0.3$) and heats rapidly giving rise to a steep temperature increase. When viewed from the fixed tube perspective, there is a steep temperature decrease for $\xi > 0.3$, i.e. in the region ahead of the torch. Alternatively, in the region behind the torch, $\xi < 0.3$, the temperature change is more gradual.

An important consideration is the effect of the torch heating from the previous pass. In the quasi-steady condition the heating (and temperature) profiles are

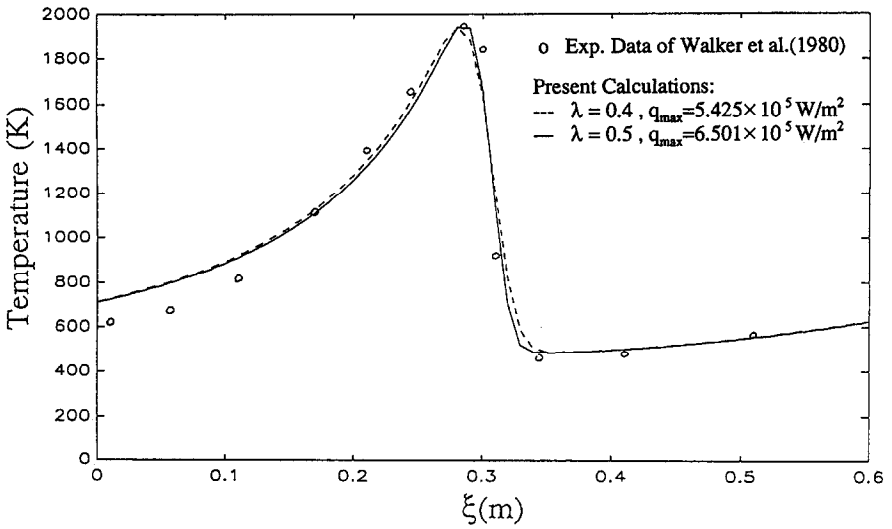

FIG. 2. Wall temperature distribution.

tied to the moving torch. The heating effects of the previous pass are clarified by the two torch concept with the tube extension. It is noted in Fig. 2 that ahead of the torch there exists a minimum wall temperature at $\xi = 0.338$. For $\xi > 0.338$ there is a gradual increase of temperature, which is the result of the torch heating from the previous pass. The two torch model of the present study correctly predicts the existence of the minimum wall temperature with the gradual increase of the wall temperature after the minimum is attained. In the present two torch concept, two torches are moving at the same speed and are separated by a distance of one tube length. The dashed torch in Fig. 1 represents the heating that occurred from the previous pass and the solid torch represents the heating from the present pass. Note that 'single' torch formulations do not yield this important minimum temperature. Ahead of the present torch ($\xi > 0.3$), the gas temperatures become higher than the wall temperature as a combined result of the convection of the heated gas and the sharp decrease of the tube wall temperature in front of the torch. Therefore, in the region ahead of the torch, the thermophoretic force directs particles to the wall. As the gas flows downstream, the gas temperature decreases; however, beyond the location of the minimum wall temperature (T_{min} in Table 1), the tube wall temperature increases and the gas temperature becomes lower than the wall temperature. The thermophoretic force is now away from the wall and the particles no longer deposit. Therefore, the location and the value of this minimum outer wall temperature have an important effect on the particle deposition [4].

The thermophoretic force is related to the temperature of the inner wall and the temperature of the gas. During deposition, the gas temperature gradient at the inner wall is negative (hot gas and cold wall). An axial location is reached where the temperature gradient becomes zero and further downstream the temperature gradient becomes positive. The solid layer results in the need to distinguish the inner wall temperature from the outer wall temperature. The thermophoretic force is clearly dependent on the inner wall temperature. Formulations that do not consider the solid layer do not have to make this distinction. The inner wall temperature, $T(r = R_i, \xi)$ which occurs at the zero gradient condition, i.e. $(\partial T/\partial r)|_{r=R_i} = 0$ is defined in this study as an equilibrium temperature T_e. It is noted in Table 1 that the difference between the T_e and the minimum temperature of the outer wall is significant. It is shown below that the use of the equilibrium temperature gives better correlation for the overall efficiency of deposition than the use of the minimum outer wall temperature. The overall deposition efficiency is numerically obtained as approximately 53% which agrees with the 56% efficiency obtained experimentally (Walker *et al.* [4]).

Parametric studies were carried out over a range of solid layer thicknesses and torch speeds for a fused silica tube (ID = 19 mm, OD = 25 mm). Calculations were made for values of the thickness of the solid layer from 3 to 4 mm, torch speeds from 10 to 20 cm min^{-1} flow rates from 2 to 4 l min^{-1} and maximum tube wall temperatures from 1800 to 2000 K. Calculations were made with the maximum wall temperature fixed and in addition, several calculations were made with the maximum heat flux fixed. A summary of the cases is given in Table 1.

Figure 3(a) shows the axial distributions of outside wall temperature for three different torch speeds when the maximum temperature is specified to be 2000 K. It is noted that in the MCVD process the tube wall temperature near the torch is monitored to be constant. For a low torch speed, the surface has a sharper temperature gradient and a lower minimum wall temperature ahead of the torch than for a high torch speed. For a low speed, the time interval between the present and the previous passes of the torch heat-

Table 1. Summary of calculation results. (A. $T_{max} = 2000$ K, B. $T_{max} = 1900$ K, C. $T_{max} = 1800$ K, D. $q_{max} = 1.2 \times 10^6$ W m^{-2})

A. $T_{max} = 2000$ K

Flowrate (l min^{-1})	Torch speed (cm min^{-1})	Inner radius (mm)	Maximum heat flux (10^6 W m^{-2})	T_{min} (K)	T_e (K)	Particle formation (%)	Tapered length (cm)	Spatial efficiency (%)
3	15	9	1.27788	519	606.5	100	24.5	47.5
2	15	9	1.28428	513	580.4	100	18	50
4	15	9	1.27372	525	628.4	62	25.5	43.2
3	10	9	0.90465	448	530.6	64	26	51.5
3	20	9	1.61918	581	675.3	100	21.5	42.9
3	15	9.5	1.14503	494	576.7	100	23.5	48
3	15	8.5	1.39796	542	632.4	100	22	45.3

B. $T_{max} = 1900$ K

Flowrate (l min^{-1})	Torch speed (cm min^{-1})	Inner radius (mm)	Maximum heat flux (10^6 W m^{-2})	T_{min} (K)	T_e (K)	Particle formation (%)	Tapered length (cm)	Spatial efficiency (%)
3	15	9	1.19272	515	600.8	66	24	47.4
2	15	9	1.19847	510	575.7	100	17.5	49.9
4	15	9	1.18898	520	672.7	40	19	39.8
3	10	9	0.84968	445	516.9	42	13.5	41.3
3	20	9	1.50428	575	667.5	100	21	42.9
3	15	9.5	1.07133	491	571.8	57	22.5	48
3	15	8.5	1.30187	537	626	80	21.5	45.2

C. $T_{max} = 1800$ K

Flowrate (l min^{-1})	Torch speed (cm min^{-1})	Inner radius (mm)	Maximum heat flux (10^6 W m^{-2})	T_{min} (K)	T_e (K)	Particle formation (%)	Tapered length (cm)	Spatial efficiency (%)
3	15	9	1.1042	511	594.8	34	9.5	33.9
2	15	9	1.10936	506	570.5	77	17.5	49.9
4	15	9	1.10082	516	614.7	21	6	20.8
3	10	9	0.79104	442	513	23	5	22.1
3	20	9	1.38638	570	659.1	50	24	44.5
3	15	9.5	1.99406	487	566.6	30	7.5	29.4
3	15	8	1.20249	533	619.1	37	11	36.8

D. $q_{max} = 1.2 \times 10^6$ (W m^{-2})

Flowrate (l min^{-1})	Torch speed (cm min^{-1})	Inner radius (mm)	Maximum heat flux (10^6 W m^{-2})	T_{min} (K)	T_e (K)	Particle formation (%)	Tapered length (cm)	Spatial efficiency (%)
3	15	9	1908	516	601.3	71	24.5	47.4
2	15	9	1903	510	575.8	100	17.5	49.9
4	15	9	1912	521	622.5	44	25.5	43.2
3	10	9	2339	456	534.1	100	26.5	51.6
3	20	9	1673	562	647.3	6	1.5	5.7
3	15	9.5	2057	496	579.4	100	23.5	48.1
3	15	8.5	1809	533	619.6	39	12.5	38.5

ing is longer; therefore, the tube is cooled for a longer time which results in a lower minimum wall temperature for the lower torch speed. The lower minimum temperature indicates that the deposition efficiency would be higher for a low torch speed as is shown in Fig. 3(b) (the lower T_{min} or T_e corresponds to larger thermophoresis). However, the percentage of particle formation should also be considered in conjunction with the particle deposition. As noted by Walker *et al.* [4], T_{min} is important in estimating the efficiency for the particle transport regime where the particle formation is high and the deposition efficiency depends on the percentage of the particles that deposit. On the other hand, for the chemical reaction regime (where the particle formation is limited to the regions near the wall), the percentage of particle formation is more important than is the percentage of particle deposition. Figure 4 shows the axial distributions of efficiency, $E(\xi)$, for different torch speeds when the maximum temperature is 1900 K. For 15

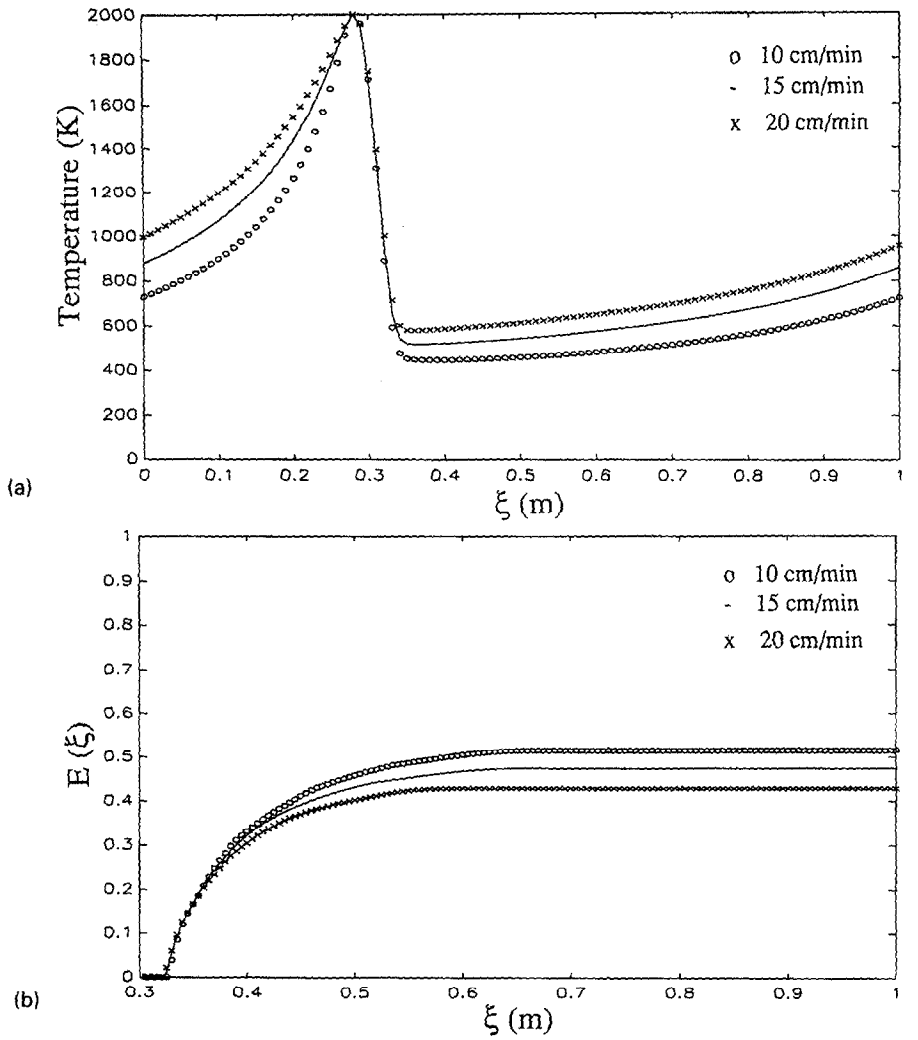

FIG. 3. (a) Axial distribution of wall temperature for various torch speeds ($T_{max} = 2000$ K, $\xi_{torch} = 0.3$ m). (b) Spatial efficiency of deposition for various torch speeds ($T_{max} = 2000$ K, $\xi_{torch} = 0.3$ m).

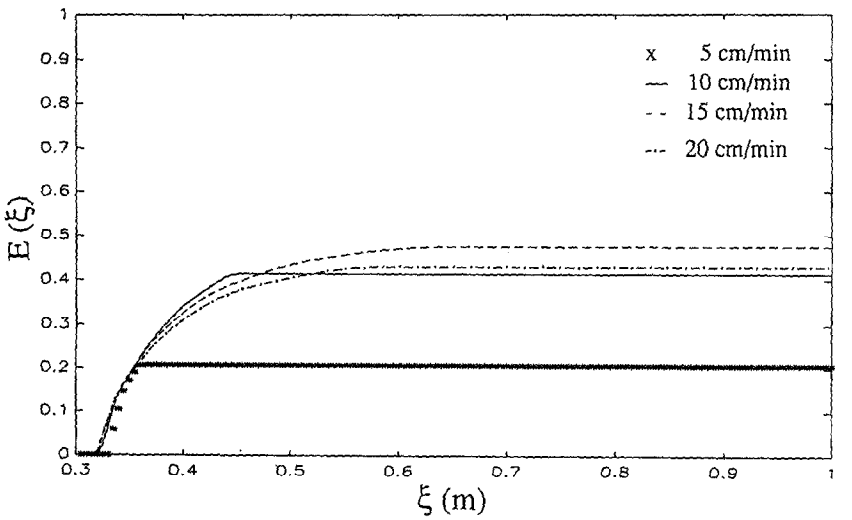

FIG. 4. Spatial efficiency of deposition for various torch speeds ($T_{max} = 1900$ K, $\xi_{torch} = 0.3$ m).

and 20 cm min^{-1} torch speeds, the particle formation is moderate and high (62 and 100%, respectively) and the efficiency depends on T_e; the slower torch case which has a lower T_e results in higher E. However, cases of $V_{torch} = 5$ and 10 cm min^{-1} show different trends, i.e. a slower torch has a lower E since a smaller percentage of particle formation occurs. This is because the wall temperatures behind the torch are lower for a lower torch speed and as a result, insufficient heating occurs and the percentage of particle formation is smaller. Another phenomenon of practical importance is the occurrence of the tapered entry; i.e. the thickness of the deposited layers varies from zero to constant value in the axial direction. Since small torch speeds give small tapered lengths, i.e. approximately 13.5 cm for 10 cm min^{-1} and 5.5 cm for 5 cm min^{-1} (Table 1), small torch speed can be utilized to reduce the tapered length albeit with the cost of lower efficiency at the initial stage of torch traversing.

As the particles deposit, the increasing thickness of the solid layer affects the heat transfer and the particle deposition. Figure 5(a) shows the distributions of the outside wall temperature for different thicknesses. The wall temperature distributions show similar shapes with the thicker wall having a slightly higher T_{min} ahead of the torch (this reduces the overall efficiency as shown in Fig. 5(b), the 4 mm thick wall has an approximately 3% lower E than the 3 mm thick wall). It is also noted that to maintain the peak temperature at 2000 K (Table 1), the maximum heat flux should be increased from 1.145×10^6 W m^{-2} for the 3 mm thick wall to 1.398×10^6 W m^{-2} for the 4 mm thick wall.

Increasing flowrates do not affect the wall temperature distributions; e.g. cases of 2, 3 and 4 l min^{-1} result in virtually identical wall temperatures. However, the flowrates do affect the deposition efficiency to some extent; in Fig. 6, it is seen that E is decreased as the flowrate increases. Higher flowrates result in higher radial temperature gradients which cause larger thermophoretic force. However, higher

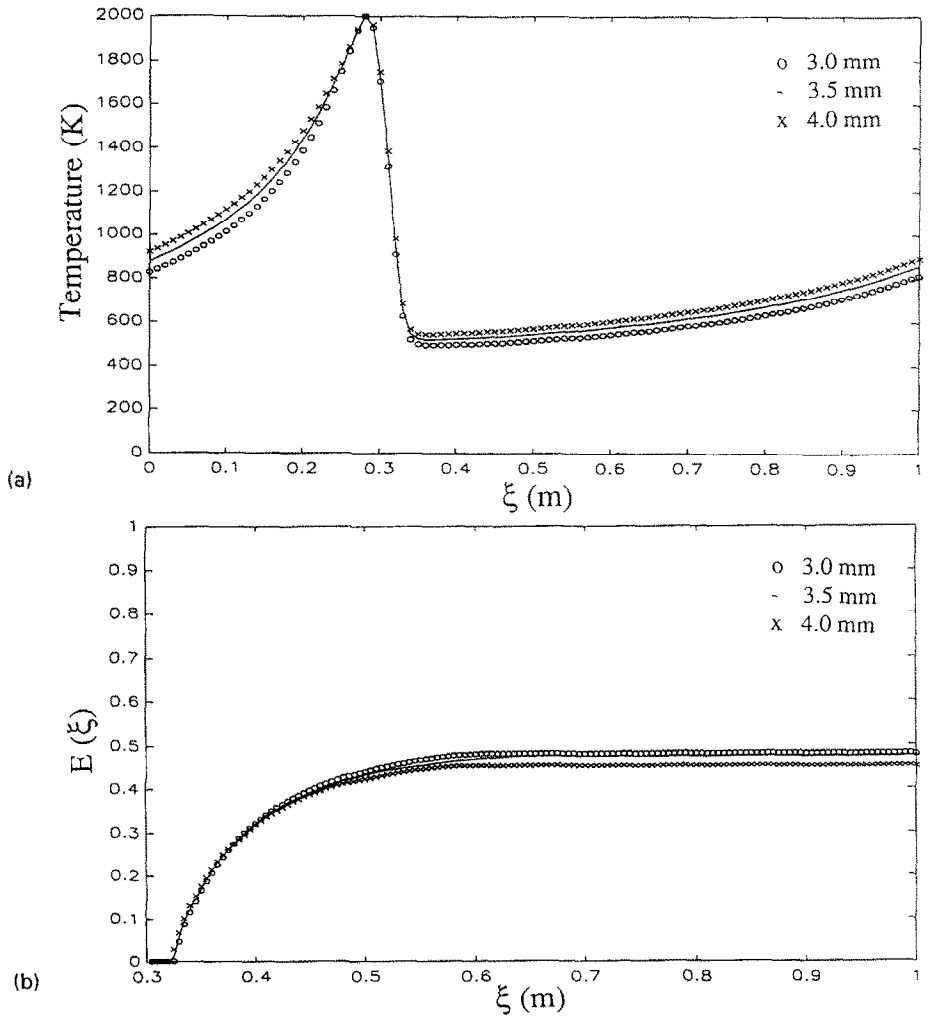

FIG. 5. (a) Axial distribution of wall temperature for various solid layer thicknesses ($T_{max} = 2000$ K, $\xi_{torch} = 0.3$ m). (b) Spatial efficiency of deposition for various solid layer thicknesses ($T_{max} = 2000$ K, $\xi_{torch} = 0.3$ m).

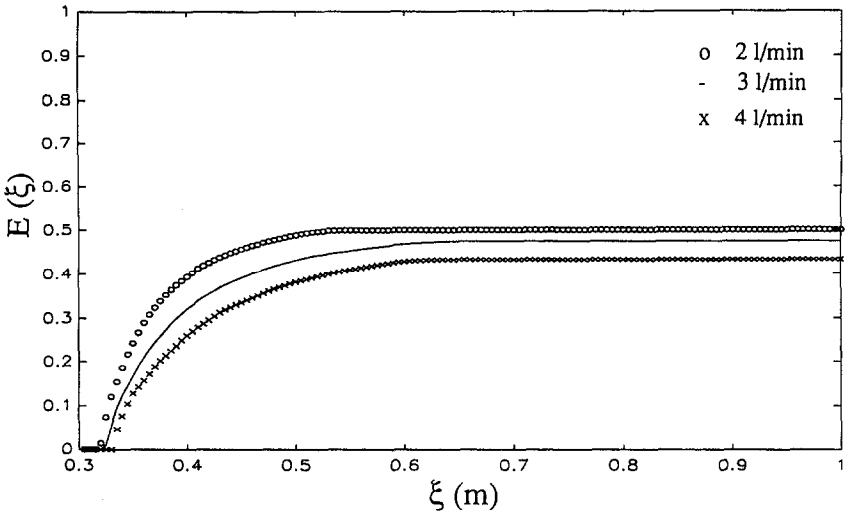

FIG. 6. Spatial efficiency of deposition for various flowrates (T_{max} = 2000 K, ξ_{torch} = 0.3 m).

gas velocity also tends to move particles out of the tube more readily. The net effect is that the higher flowrate case results in a lower efficiency of particle deposition. However, the smaller efficiency for the higher flowrate does not necessarily mean a smaller rate of deposition because the rate of deposition is proportional to E times the flow rate. Figure 7 shows the deposition rate/F where F is the conversion ratio in gram l^{-1} from $SiCl_4$ to SiO_2. Note that a flowrate exists that yields the maximum rate of particle deposition. The flowrate that yields the maximum rate will be approximately 4 and 2 l min^{-1} for T_{max} = 1900 and 1800 K, respectively, and would be higher than 4 l min^{-1} for T_{max} = 2000 K.

Figure 8 shows the variations of the tube wall temperature for different torch speeds for the case of the fixed maximum heat flux. There exists a significant variation of the peak temperatures and axial distributions which would result in different deposition profiles. For the fixed maximum heat flux, the results for different thicknesses of the solid layers show similar trends, i.e. large variations of temperatures and deposition profiles (not presented). Therefore, maintaining the peak temperature per one pass of the torch traverse is important to obtain uniformity of deposition.

For high formation of particles (particle transport regime defined by Walker *et al.* [4]), the overall efficiency is closely related to the minimum wall temperature ahead of the torch. Figure 9 shows a strong correlation among the formula suggested by Walker *et al.* [4], the present fitting formulas and the calculations. Blank circles represent the results for the minimum outside wall temperatures and the efficiencies and the solid circles represent the results for the equilibrium temperature T_e (defined as a inner tube wall

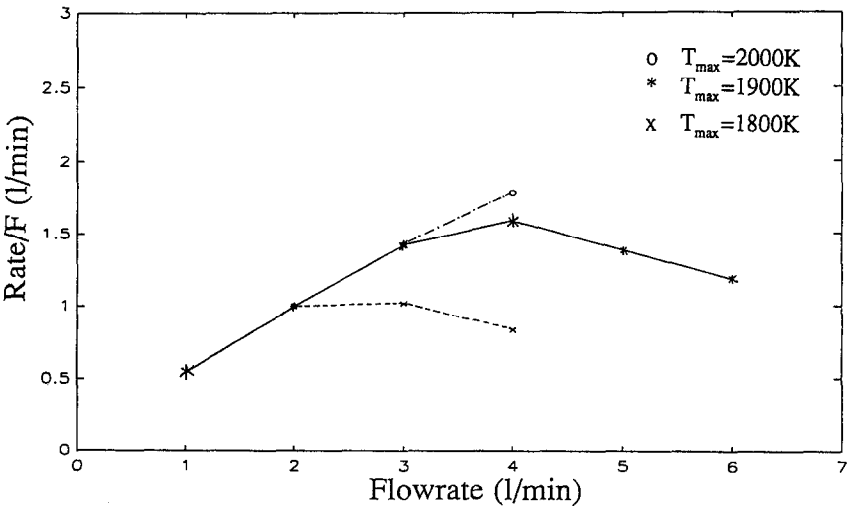

FIG. 7. Deposition rate for different flowrates.

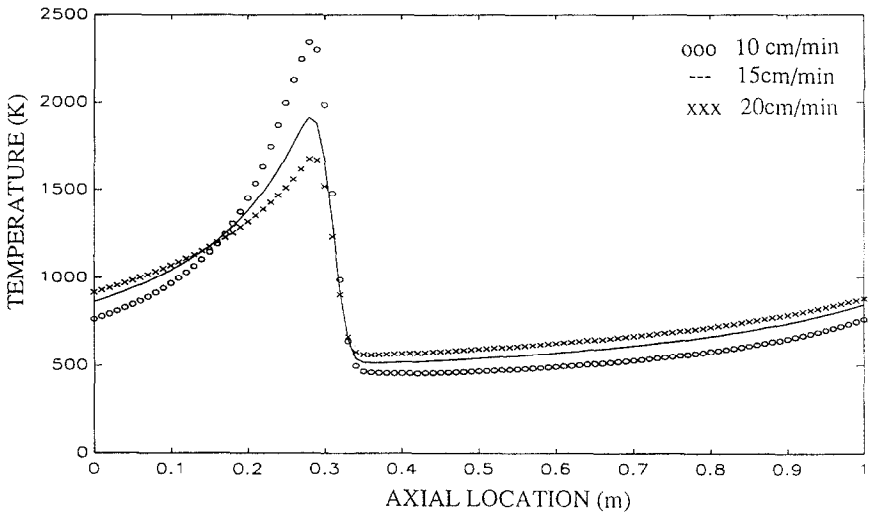

FIG. 8. Axial distribution of wall temperature for various torch speeds (Q_{max} = constant, ζ_{torch} = 0.3 m).

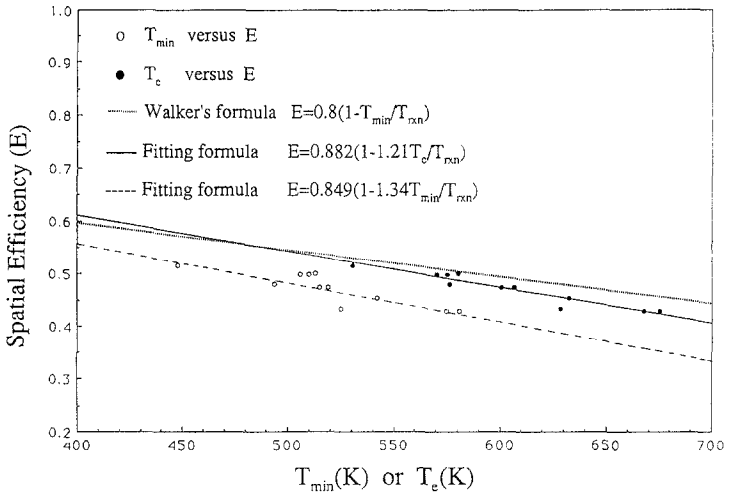

FIG. 9. Efficiency correlation among minimum, equilibrium temperatures and formulas.

temperature to satisfy $(\partial T/\partial r)|_{r=R_1} = 0$) and the efficiencies. The formula given by Walker *et al.* [4] shows a better agreement with the solid circles which uses the equilibrium temperatures. The two fitting formulas which use the minimum outer wall temperature and the equilibrium temperature, respectively are suggested for a better agreement.

SUMMARY AND CONCLUSIONS

An analysis of the effects of torch speed and solid layer thickness on the efficiency, the rate of particle deposition and the tapered length has been carried out for the Modified Chemical Vapor Deposition process. A new concept which uses a two torch formulation and the heat flux boundary condition is utilized to simulate torch heating from both the present and the previous passes. The effects of the increasing solid layer thickness are also studied.

The numerical results were compared with the experimental data of wall temperature distribution and deposition efficiency and shown to be in good agreement. The two torch concept is able to predict the minimum wall temperature ahead of the torch which is closely related to the overall deposition efficiency. For the case of the fixed maximum wall temperature of 2000 K, the wall temperature gradient becomes sharper and the overall efficiency increases as the torch speed decreases. For T_{max} = 1900 K, small torch speed cases correspond to the chemical reaction limited regime and the efficiency decreases as the torch speed decreases from 10 to 5 cm min^{-1}.

The increasing thickness of the solid layer slightly decreases the efficiency (a 3% reduction for a 1 mm

thickness increase). A flow rate exists that yields a maximum rate of particle deposition although the efficiency of particle deposition decreases as the flow rate increases. For $T_{max} = 1900$ K and $V_{torch} = 15$ cm min^{-1}, approximately 4 l min^{-1} flow rate resulted in the maximum rate of deposition.

Acknowledgements—Support from the Korea Science and Education Foundation (Grant no. : 921-0900-004-2) is gratefully acknowledged.

REFERENCES

1. J. B. MacChesney, P. B. O'Connor and H. M. Presby, A new technique for preparation of low loss and graded index optical fibers, *Proc. IEEE 62*, pp. 1278–1279 (1974).
2. J. B. MacChesney, P. B. O'Connor, F. V. DiMarcello, J. R. Simpson and P. D. Lazay, Preparational low loss optical fibers using simultaneous vapor phase deposition and fusion, *Proc. 10th Int. Congr. Glass*, Kyoto, Japan, pp. 6-40–6-44 (1974).
3. S. R. Nagel, J. B. MacChesney and K. L. Walker, An overview of Modified Chemical Vapor Deposition process and performance, *IEEE J. Quantum Electronics*, Vol. QE-18, No. 4, pp. 459–476 (1982).
4. K. L. Walker, F. T. Geyling and S. R. Nagel, Thermophoretic deposition of small particles in the MCVD process, *J. Am. Ceram. Soc.* **63,** 552–558 (1980).
5. P. G. Simpkins, S. G. Kosinski and J. B. MacChesney, Thermophoresis: the mass transfer mechanism in MCVD, *J. Appl. Phys.* **50,** 5676–5681 (1979).
6. C. Y. Wang, T. F. Morse and J. W. Cipolla, Jr, Laser induced natural convection and thermophoresis, *ASME J. Heat Transfer* **107,** 161–167 (1985).
7. T. F. Morse, D. DiGiovanni, Y. W. Chen and J. W. Cipolla, Jr., Laser enhancement of thermophoretic deposition processs, *J. Lightwave Technol.* **LT-4**(2), 151–155 (1986).
8. K. S. Kim and S. E. Pratsinis, Manufacture of optical waveguide preforms by MCVD, *A.I.Ch.E. J.* **34,** 912–920 (1988).
9. M. Choi, Y. T. Lin and R. Greif, Analysis of buoyancy and tube rotation relative to the Modified Chemical Vapor Deposition process, *ASME J. Heat Transfer* **111,** 1031–1037 (1989).
10. Y. T. Lin, M. Choi and R. Greif, A three dimensional analysis of the flow and heat transfer for the MCVD process including buoyancy, variable properties and tube rotation, *ASME J. Heat Transfer* **113,** 400–406 (1991).
11. Y. T. Lin, M. Choi and R. Greif, A three dimensional analysis of particle deposition for the Modified Chemical Vapor Deposition (MCVD) process, *ASME J. Heat Transfer* **114,** 735–742 (1992).
12. R. C. Weast and M. J. Astle, *CRC Handbook of Chemistry and Physics* (61st Edn). CRC Press, Boca Raton, Fl (1981).
13. T. F. Irvine and P. E. Liley, Jr., *Steam and Gas Tables with Computer Equations*, pp. 161–165. Academic Press, New York (1984).
14. B. Farouk and K. S. Ball, Convective flows around a rotating isothermal cylinder, *Int. J. Heat Mass Transfer* **28,** 1921–1935 (1985).
15. R. Gardon, A review of radiant heat transfer in glass, *J. Am. Ceramic Soc.* **44**(7), 305–312 (1961).
16. U. C. Paek and R. B. Runk, Physical behavior of the neck-down region during furnace drawing of silica fibers, *J. Appl. Phys.* **49**(8), 4417–4422 (1978).
17. G. M. Homsy and K. L. Walker, Heat transfer in laser drawing of optical fibers, *Glass Technol.* **20**(1), 20–26 (1979).
18. R. Siegel and J. R. Howell, *Thermal Radiation Heat Transfer* (2nd Edn), pp. 497–516. McGraw-Hill, New York (1981).
19. S. V. Patankar, *Numerical Heat Transfer and Fluid Flow*. Hemisphere, New York (1980).
20. Y. T. Lin, M. Choi and R. Greif, An analysis of the effect of the solid layer for the Modified Chemical Vapor Deposition process, *Wärme und Stoffübertragung* **28,** 169–176 (1993).